Electron-Induced Decomposition of Solid 1,1-Diamino-2,2-Dinitroethylene (FOX-7) at Cryogenic Temperatures

Andrew M. Turner,[a,b] Joshua H. Marks,[a,b] Yuheng Luo,[a] Jasmin T. Lechner,[c] Thomas M. Klapötke,[c] Rui Sun,[a] Ralf I. Kaiser [a,b*]

[a] *Department of Chemistry, University of Hawaii, Honolulu, HI 96822, USA*

[b] *W. M. Keck Research Laboratory in Astrochemistry, University of Hawaii, Honolulu, HI 96822, USA*

[c] *Department of Chemistry, Ludwig-Maximilian University of Munich, 81377 München, Germany*

*ralfk@hawaii.edu

ABSTRACT

Solid FOX-7 (1,1-diamino-2,2-dinitroethylene), an energetic material of interest due to its high stability and low shock/thermal sensitivity, was exposed to energetic electrons at 5 K to explore the fundamental mechanisms leading to decomposition products and provide a better understanding of the reaction pathways involved. As a result of the radiation exposure, infrared spectroscopy revealed carbon dioxide (CO_2) and carbon monoxide (CO) trapped in the FOX-7 matrix, while these compounds along with water (H_2O), nitrogen monoxide (NO), and cyanogen (C_2N_2) were detected exploiting quadrupole mass spectrometry both during irradiation and during the warming phase from 5 K to 300 K. Photoionization reflectron time-of-flight mass spectrometry (PI-ReTOF-MS) detected small molecules such as ammonia (NH_3), nitrogen monoxide (NO), and nitrogen dioxide (NO_2) as well as more complex molecules up to 96 amu. Potential reaction pathways are presented and assignments are discussed. Among the reaction mechanisms, the importance of an initial nitro-to-nitrite isomerization is highlighted by the observed decomposition products.

1. INTRODUCTION

An understanding of the stability,[1-2] explosion efficiency,[3-4] and shock/thermal sensitivity of energetic materials such as FOX-7 (1,1-diamino-2,2-dinitroethylene) (Scheme 1) is critical to access the potential of novel compounds as safe and effective energetic materials.[5-11] Investigations into the decomposition mechanisms of FOX-7 and the subsequent reactions of newly generated radical species are challenging[12] due to the non-equilibrium conditions of these reactions that result in excess kinetic and internal energy[13] capable of overcoming reaction entrance barriers.[14] Traditional explosives such as RDX (1,3,5-trinitro-1,3,5-triazine) and HMX (octahydro-1,3,5,7-tetranitro-1,3,5,7-tetrazocine), as well as the explosives of interest octanitrocubane and CL-20 (hexanitrohexaazaisowurtzitane),[15-16] all possess cyclic structures with nitro moieties ($-NO_2$), while FOX-7 is an acyclic molecule that also contains amino groups (NH_2) that provide more complex decomposition pathways. As a relatively new molecule that was first synthesized in 1998,[17] experimental and computational results on the decomposition of FOX-7 are not converging.

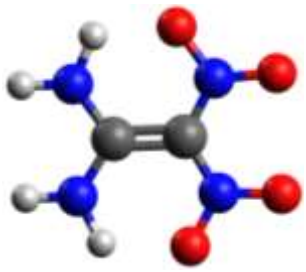

Scheme 1: 1,1-diamino-2,2-dinitroethylene (FOX-7)

Nitric oxide (NO) has been identified as a principle product in gas-phase experimental studies with theoretical support suggesting that NO evolves from nitro-to-nitrite isomerization[18] with isomerization barriers from 244[19] to 247[20] kJ mol^{-1}. After NO loss, this decomposition yields the $(NH_2)_2CC(O)NO_2$ radical.[20] A hydrogen shift to $H_2N(NH)CC(O)NOOH$ can be followed by elimination of nitrous acid (HONO); the $H_2N(NH)CCO$ fragment can further decompose to hydrogen isocyanide (HNC), the amino radical (NH_2), and carbon monoxide (CO). Computations have focused on the weak C–NO_2 bond as a starting point to decomposition[21] and found dissociation energies of 280,[22] 290,[19] 293,[23] 297,[24] 300,[25] and 301 kJ mol^{-1};[26] these energies contrast the strong C-NH_2 bond[18] with dissociation energies of 461,[25] 467,[23] and 503 kJ mol^{-1}.[22] A temperature dependence of these reactions was found such that the C–NO_2 bond cleavage should be the predominate pathway above 250 K, while nitro-to-nitrite isomerization is only possible up to 500 K.[27] Molecular dynamics simulations at 3,000 K suggest that the initial C–NO_2 bond cleavage occurs within 10 ps producing nitrogen dioxide (NO_2) and eventually molecular nitrogen (N_2) and water (H_2O).[28] Additionally, hydrogen migration to the nitro group (NO_2) leads to elimination of nitrous acid (HONO). Further studies clarified these findings and revealed that the competing C–NO_2 bond cleavage and nitro-to-nitrite isomerization pathways are influenced by electronic excitation and charge-trapping that favors C–NO_2 bond cleavage.[22] Contrary to the previous studies, this report [20] proposed that hydrogen transfer processes were insignificant in the gas phase, but could play an important role in condensed phase decomposition as confirmed in later studies.[29] Unfortunately, multiple calculations only consider isolated gas-phase molecules under collision-less conditions, while the actual crystalline environment of FOX-7 can dramatically influence reaction energies and barriers due to π-π stacking and hydrogen bonding.[30]

Solid FOX-7 thermally decomposes around 500 K producing several oxides of nitrogen: nitric oxide (NO), nitrous oxide (N_2O), dinitrogen trioxide (N_2O_3), nitrogen dioxide (NO_2), and nitrous acid (HONO) along with water (H_2O), carbon monoxide (CO), carbon dioxide (CO_2), ammonia (NH_3),

hydrogen cyanide (HCN), cyanic acid (HOCN), isocyanic acid (HNOCO), and formic acid (HCOOH).[31-32] Experiments utilizing laser-induced breakdown spectroscopy detected NO, NO_2, HONO, formaldehyde (H_2CO), and acetylene (C_2H_2),[33] while time-resolved Raman spectroscopy was employed to investigate shock-compressed FOX-7.[34] In the condensed phase, the production of nitrous acid (HONO) and water (H_2O) can result from hydrogen abstraction by nitrogen dioxide (NO_2) and the hydroxyl radical (OH).[35] To better understand the decomposition of FOX-7 and to investigate additional energetic materials, derivatives of and mixtures with FOX-7 have been recently investigated. Li et al. considered mixtures of FOX-7 with H_4TPP (2,3,5,6-tetra(1H-tetrazol-5-yl)pyrazine) using density functional theory (DFT) and molecular dynamics simulations.[36] The addition of FOX-7 to CL-20 (hexanitrohexaazaisowurtzitane) and HMX (1,3,5,7-tetranitro-1,3,5,7-tetrazocane) resulted in co-crystals with high thermal stabilities and improved impact sensitivity,[37-38] demonstrating safer, but still powerful explosives can result from mixtures compared to individual compounds. Krisyuk and Sypko computationally investigated FOX-7 derivatives with one or two hydrogens replaced by amino (NH_2) groups and found the main thermolysis channel of the derivative involves hydrogen transfer to a carbon atom with subsequent elimination of NO_2 and HONO without the *aci*-form transformations observed in FOX-7 after the hydrogen transfer.[39] Further studies using diazacyclic derivatives that bridge the amino groups of FOX-7 found similar initial decomposition paths as FOX-7 when considered computationally.[40] This is in agreement with experimental evidence of FOX-7 and diazacyclic derivatives in dilute solution with nitrobenzene ($C_6H_5NO_2$), but was in contrast to solid samples that partially liquefied during thermolysis and generated products with catalytic capabilities that resulted in much faster decomposition compared to the solution phase.[41]

The aforementioned studies indicate that a complete understanding of the decomposition of condensed-phase FOX-7 under various temperatures and conditions remains unclear, especially compared to gas-phase computational results. This is due to the increased complexity of solid state decomposition pathways that have a greater number of possible intermediates and products relative to predicted gas-phase processes. The close proximity of radical intermediates constrained in a condensed phase 'matrix cage' also results in a sequence of reactions not possible in the gas phase; this has been observed in studies of other energetic materials such as RDX (1,3,5-trinitroperhydro-1,3,5-triazine).[15-16] In order to fully understand the numerous possible intermediates, reaction mechanisms, and products that can occur in the condensed phase, experimental investigations of solid FOX-7 under various decomposition conditions are necessary. In order to determine the dominating reaction mechanisms

that provide the source of non-thermal radicals that lead to the decomposition of energetic materials, the decomposition of solid FOX-7 was investigated at 5 K.[42] At 5 K, the photolysis of this cooled sample revealed that nitric oxide (NO) evolved from 355 nm photolysis, while molecular oxygen (O_2) was also detected using both 355 nm and 532 nm photons with branching ratios of NO to O_2 found to be 700:1 at 355 nm. These results provided a crucial first step in understanding the initial decomposition reactions of solid FOX-7 and dubbed FOX-7 as an explosive 'delivering its own oxidant', but were restricted to the low photon energy; this in turn inhibited the generation of higher order products.

Here, in the present work, solid FOX-7 at 5 K was processed by low energy electrons[43-44] generated in the track of energetic electrons, with sufficient energy capable of cleaving bonds of FOX-7 molecules and overcoming reaction barriers to induce non-equilibrium chemistry toward higher order products pertinent to the decomposition of this energetic material. The experimental design monitored the changes to the solid FOX-7 *in situ* using Fourier transform infrared spectroscopy (FTIR) while gaseous products that sublime from the sample at 5 K and in the temperature programmed desorption (TPD) process were detected using two complementary mass spectrometric techniques: electron-impact quadrupole mass spectrometry (EI-QMS) and single photon photoionization reflectron time-of-flight mass spectrometry (PI-ReTOF-MS). While both methods utilize mass-to-charge ratios and sublimation temperatures to determine the identity of subliming molecules, the more sensitive soft PI-ReTOF-MS technique[45-46] also exploits ionization energies (IEs) to provide additional data for assigning both molecules and isomers. Using these complementary techniques, the decomposition of solid FOX-7 can be explored to elucidate key products and reaction mechanisms as performed in the present study.

2. EXPERIMENTAL SECTION

FOX-7 samples with a thickness of 2.0 ± 0.5 μm about were prepared by dispensing dropwise a dilute solution of FOX-7 in dimethyl sulfoxide (DMSO) onto a polished silver wafer and evaporating under vacuum.[42] FOX-7 was synthesized according to the procedure described by Laytpov et al. and Astrat'ev et al.[42,47-48] The wafer was interfaced to a copper cold head in a stainless steel ultrahigh vacuum chamber with operating pressures less than 1×10^{-10} Torr. Samples were cooled to 5 K using a two-stage helium refrigerator (Sumitomo Heavy Industries) and then warmed to 320 K at 1 K min^{-1} to release any residual DMSO trapped in the FOX-7 matrix. The sample was then cooled back to 5 K and irradiated with 5 keV electrons for 60 minutes at 500 nA current resulting in a flux of 3.1×10^{12} electrons s^{-1} cm^{-2} or 2.5×10^{-3} W cm^{-2}. The irradiated sample was then heated to 300 K at 1 K min^{-1} to establish a temperature programmed desorption (TPD) protocol. As the sample was warmed, the

subliming product molecules were detected using reflectron time-of-flight mass spectrometry (ReTOF-MS, Jordan TOF Products) utilizing 10.49 eV vacuum ultraviolet (VUV) photons (118 nm) for photoionization (PI). The 10.49 eV photons are the ninth harmonic of a Nd:YAG laser (Spectra Physics PRO 250, 30 Hz) and are generated by tripling the third harmonic output (355 nm) using non-resonant four-wave mixing ($3\nu_1 = \nu_{VUV}$) with pulsed xenon gas as the non-linear medium.[49] The photoionized molecules were detected by a dual multichannel plate, after which the signals were amplified (Ortec 9305) and recorded by a FAST ComTec MCS6A multichannel scalar operating at 30 Hz (Quantum Composers 9518). An electron-impact (EI, 70 eV) quadrupole mass spectrometer (QMS) operating as a residual gas analyzer (RGA) was also employed and, although much less sensitive than the ReTOF-MS system, was useful for detecting molecules with ionization energies above 10.49 eV that would not be ionized and detected with the ReTOF-MS. In addition, Fourier-transform infrared spectroscopy (FTIR, 500–6000 cm^{-1}, 4 cm^{-1} resolution) probed the sample during irradiation to observe both changes to FOX-7 and new molecules frozen in the sample awaiting sublimation during TPD. The penetration depth of the electrons was calculated using CASINO simulations (Figure 1),[50] which found that 99 % of the electron energy was absorbed in the top 350 nm sample layers. This results in an average dose of 210 eV $molecule^{-1}$.

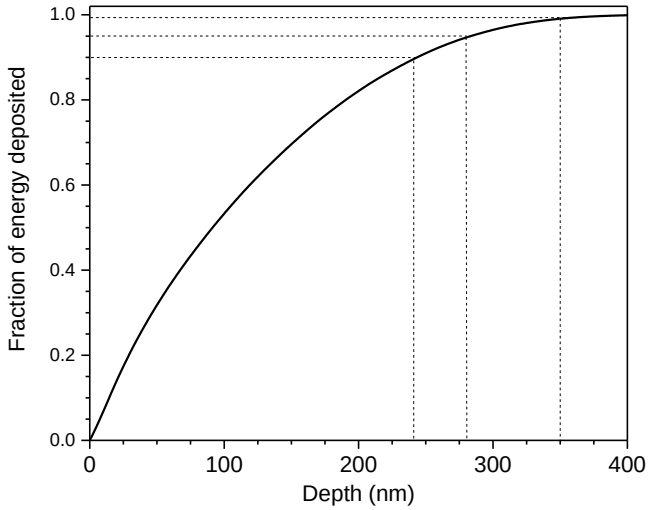

Figure 1. Fraction of deposited electron energy as a function of depth. The dashed lines indicate that 90 % of the energy is deposited in the upper 240 nm, 95 % is deposited at 280 nm, and 99 % at 350 nm.

3. RESULTS

Infrared Spectroscopy

The infrared spectrum recorded before the irradiation displays prominent absorptions consistent with previous works (Table S1, Figure 2).[42] The highest energy fundamentals (ν_1–ν_4) belong to NH_2 stretching vibrations (3442–3313 cm^{-1}) and exist in an isolated region separate from the dense 1650–600 cm^{-1} region of peaks assigned to ν_5– ν_{24}. Additional vibrations of the NH_2 group include scissoring (ν_6, 1606 cm^{-1}; ν_7, 1525 cm^{-1}), rocking (ν_{11-16}, 1311–1038 cm^{-1}), and twisting (ν_{18}, 771 cm^{-1}; ν_{20}, 737 cm^{-1}; ν_{21}, 679 cm^{-1}; ν_{24}, 623 cm^{-1}). Besides NH_2 vibrations, ν_{11}, ν_{12}, ν_{20}, and ν_{21} can also be assigned to C–NO_2 vibrations while ν_{13} and ν_{14} can also be assigned to symmetric stretching of the NO_2 group. The asymmetric stretch of the NO_2 group occurs at 1352 cm^{-1} (ν_{10}) and scissoring modes are seen at 862 cm^{-1} (ν_{17}) and 748 cm^{-1} (ν_{19}). Carbon-carbon stretching is observed at 1498 cm^{-1} (ν_8) and 748 cm^{-1} (ν_{19}). The final fundamental vibration (1649 cm^{-1}, ν_5) is assigned to C–NH_2 stretching.

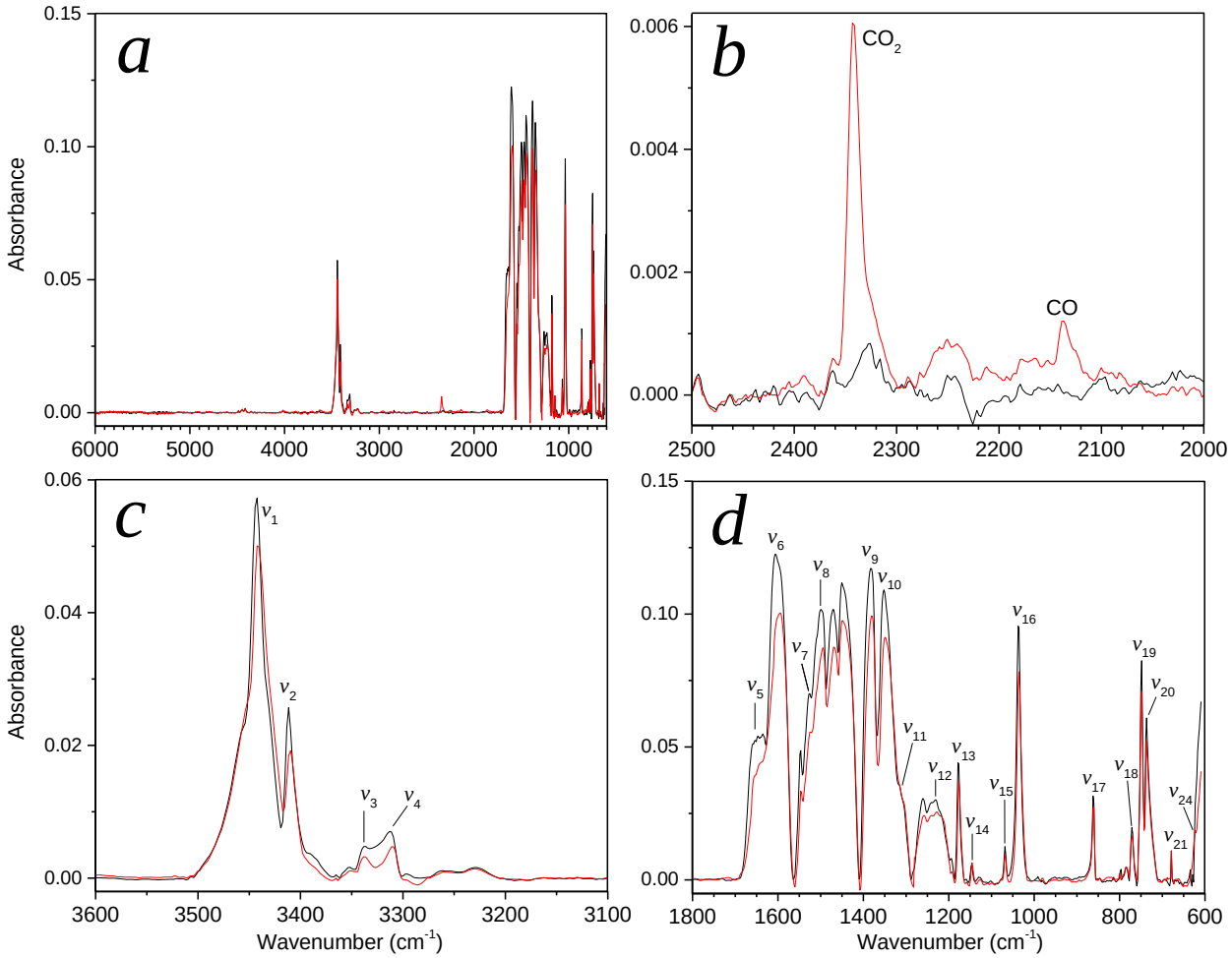

Figure 2. Infrared spectra of solid FOX-7 taken before (black) and after (red) irradiation. a) Full spectral range, b) Spectral region highlighting carbon dioxide (CO_2) and carbon monoxide (CO) vibrations that appeared during irradiation, c) Region displaying ν_1– ν_4, d) Region displaying ν_5– ν_{24}

After the irradiation, only two new peaks were identified: 2343 cm^{-1} for carbon dioxide (CO_2, ν_4) and 2137 cm^{-1} for carbon monoxide (CO). Figure 3 displays the increase of these absorption bands during irradiation using absorption coefficients of 7.3×10^{-17} cm $molecule^{-1}$ for CO_2 and 1.1×10^{-17} cm $molecule^{-1}$ for CO to calculate column densities.[51] Ultimately, $1.5 \pm 0.2 \times 10^{15}$ molecules of CO_2 and $1.2 \pm 0.2 \times 10^{15}$ molecules of CO were generated during the irradiation based on these infrared absorption bands. These data were also fit with first-order rate constants to obtain $k_{CO2} = 1.3 \times 10^{-4}$ s^{-1} and $k_{CO} = 3.5 \times 10^{-4}$ s^{-1}, respectively.

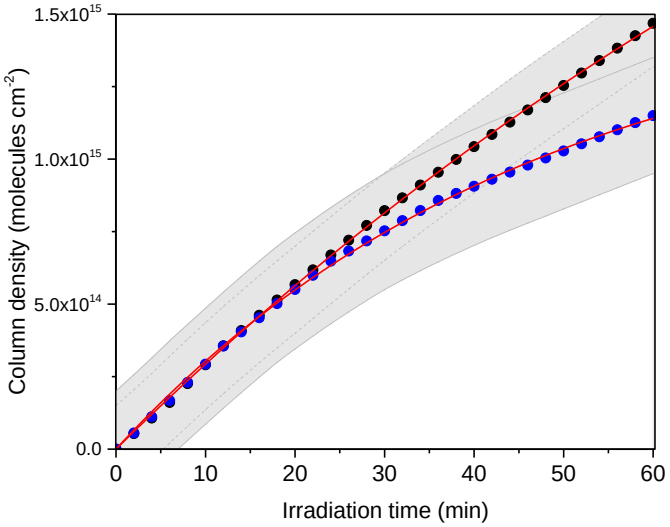

Figure 3. Increases in column densities of carbon dioxide (CO_2, black) and carbon monoxide (CO, blue) within the FOX-7 sample during irradiation. The red lines display fitting with first-order rate constants.

Besides the newly emerging absorptions, Figure 4 also reveals prominent declines of peaks associated with FOX-7 for the C=C (ν_9), NO_2 (ν_{10}), and NH (ν_{1-4}) functional groups. The data reveal overall (pseudo) first order decays with rate constants of $k_{C=C} = 6.8 \times 10^{-4}$ s^{-1}, $k_{NO2} = 1.3 \times 10^{-3}$ s^{-1}, and $k_{NH} = 2.1 \times 10^{-3}$ s^{-1}. Each graph demonstrates that about 84 % of the functional groups remain intact after the irradiation indicating that 16 % of the FOX-7 molecules reacted. Given that the sample is 2 μm thick, 16 % of the molecules would occupy a layer 320 nm thick. According to the CASINO simulation, 98 % of the electron energy is absorbed in the top 320 nm, which demonstrates the CASINO calculations are in excellent agreement with the diminished infrared band intensities. Using the density

of FOX-7 (1.89 g cm^{-3}), this 320 nm layer would contain 2.5×10^{17} molecules of FOX-7. The conversion of the 5×10^{17} carbon atoms – one FOX-7 contains two carbon atoms - to CO and CO_2 results in a very low yield of the terminal oxidation products of only 0.2 % for CO and 0.3 % for CO_2.

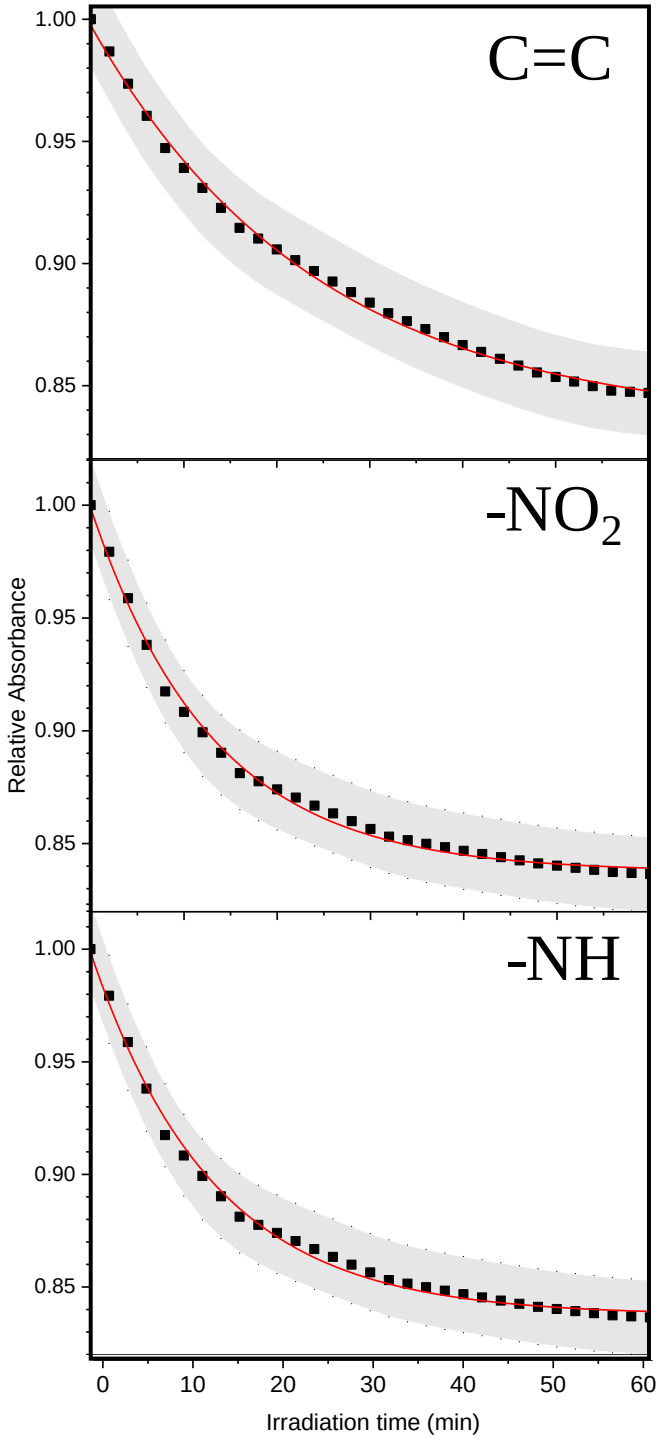

Figure 4. Infrared intensities for three functional groups of FOX-7 (C=C, -NO_2, and -NH) relative to their pre-irradiation starting values. The plots show that about 84 % of the functional groups remain after irradiation. Red lines indicate fitting using first-order rate constants.

Quadrupole Mass Spectrometry

The TPD profiles for observed QMS signals are presented in Figure 5. Consistent with the FTIR data, CO (m/z = 28) and CO_2 (m/z = 44) were detected. During TPD, carbon dioxide begins subliming at 125 K and peaks at 150 K before declining to baseline at 190 K. This sublimation is at significantly higher temperatures than in pure or mixed carbon dioxide ices, which peak from 90–95 K[52-54]. This finding indicates that CO_2 is trapped within the irradiated FOX-7 matrix. Carbon monoxide has an initial peak at 35 K, which is an expected temperature in ice experiments, but also shows signal beginning at 130 K that peaks at 165 K and 180 K. This later signal does not arise from fragmentation of CO_2 in the QMS as calibration experiments determined that, when pure CO_2 was introduced to the QMS, the observed m/z = 28 signal was only 8 % of the m/z = 44 signal and thus could not explain the high abundance of m/z = 28 in the TPD profile. Additional ions observed in the QMS include m/z = 18, which peaks at 180 K and is assigned to water, and m/z = 30, which also peaks near 180 K and belongs to nitric oxide (NO). Previous experiments of FOX-7 irradiated with 532 nm and 355 nm photons also detected NO in the QMS, but did not observe CO nor CO_2. Instead, molecular oxygen (O_2, m/z = 32) was detected after photolysis, but this product was not detected using electron irradiation; this suggests that 532 nm or 355 nm photons do generate O_2. In contrast, energetic electrons create CO and CO_2, which are classical ‘terminal combustion products’ of carbon-based molecules with O_2; this result suggests that O_2 may have formed, but sufficient energy was available to allow O_2 to react with the FOX-7. In addition to H_2O, CO, NO, and CO_2, the final product observed in the QMS appears at m/z = 52 and is best assigned to cyanogen (NCCN), which has a similar TPD profile to H_2O and NO with a peak near 180 K.

Not only were products observed subliming during TPD, but a substantial amount of products was detected by the QMS during irradiation. The irradiation profiles shown in Figure 5 show that the signals slowly increase after irradiation commences. The signals for CO and CO_2 rise most rapidly, requiring about 6 minutes to plateau, while H_2O and NCCN had the slowest rises and took 12–15 minutes to stabilize. The profiles followed the same general trend with an initial maximum followed by a decline

midway through irradiation then ending with a region of highest intensity. Once irradiation ended, H_2O and NCCN, and to a lesser extent NO, began to slowly decline and took up to 15 minutes to reach baseline. Interestingly, the CO and CO_2 signals remained high for 3–4 minutes after irradiation stopped suggesting 'outgassing' then rapidly declined, reaching baseline in about 5 minutes.

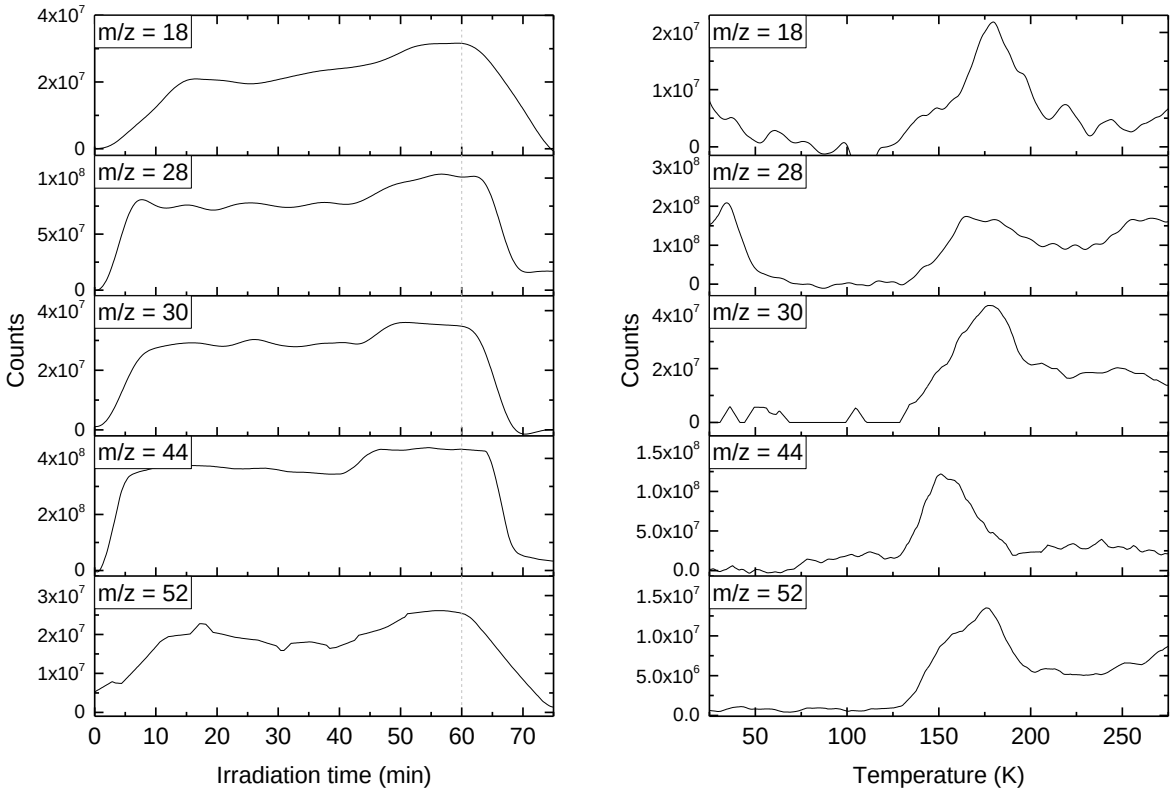

Figure 5. Mass spectra profiles recorded using the QMS showing signals that evolved during irradiation (left) and during TPD (right). The dashed line indicates the end of the irradiation.

In order to quantify the number of detected molecules, the integrated signals during irradiation and TPD can be compared with calibration experiments and ionization cross sections. The calibration experiments were performed by condensing 120 nm over 1 cm^2, determined using laser interferometry,[55] of CO_2 or NO and performing a TPD to record the number of QMS counts to compare them with the number of molecules in the 1.2×10^{-5} cm^3 ice. Since the parent peaks of the calibration signal saturated the detector, signals for m/z = 45 ($^{13}CO_2$) and m/z = 31 (^{15}NO) were utilized and corrected for their natural isotopic abundance. The calibration established a molecule-to-signal ratio (K) of 5.0×10^5 for K_{CO2} and 4.2×10^5 for K_{NO}, meaning that about one in every 5×10^5 subliming

molecules is detected. These conversion factors can be applied to the remaining products by accounting for differences in ionization cross sections [56] to obtain $K_{CO} = 5.8 \times 10^5$ and $K_{H2O} = 6.5 \times 10^5$, while $K_{(CN)2}$ is determined to 3.5×10^5. Using these conversion factors, 1.4×10^{15} molecules of CO and 1.7×10^{15} molecules of CO_2 sublimed during TPD, which are 10–15% higher than the values calculated using FTIR; therefore, these data show reasonable agreements between both QMS and FTIR methods. Using the total counts for CO, CO_2, and $(CN)_2$, 4.0 % of the 5×10^{17} carbon atoms in the reaction region sublimed during irradiation or TPD; about 96 % of the carbon from the decomposed FOX-7 remained on the sample as non-volatile products.

Reflectron time-of-flight mass spectrometry

Utilizing ReTOF-MS proved to be a more sensitive detection method compared to QMS as products with up to m/z = 96 were observed (Figure 6). However, only molecules with an ionization energy (IE) less than 10.49 eV can be observed using PI-ReTOF-MS and thus H_2O (IE = 12.62 eV), CO (IE = 14.01 eV), CO_2 (IE = 13.78 eV), and NCCN (IE = 13.37 eV), which were detected using QMS, cannot be ionized and hence are undetectable with PI-ReTOF-MS. The only exception is NO (IE = 9.26 eV), which can be probed using both methods. Not surprisingly, NO provided the most intense signal detected by ReTOF-MS and began subliming at 135 K; the ion counts reached the peak at 177 K followed by a second peak from 247–257 K. The only lower-mass product than NO seen by the ReTOF was at m/z = 17 and can be assigned to ammonia (NH_3). Ammonia's high sublimation temperature that begins at 239 K and peaks at 287 K suggests that ammonia is strongly bound to the FOX-7 matrix through intermolecular forces such as hydrogen bonding. Another small molecule observed by ReTOF was nitrogen dioxide (NO_2) at m/z = 46. Nitrogen dioxide has been a frequently reported decomposition product of FOX-7[21,31,33] and has been predicted computationally.[19,26,28,35] The sublimation of NO_2 begins at 135 K and progresses through a smaller peak at 165 K before reaching the highest peak at 177 K. As mass-to-charge ratios increase beyond those of simple molecules, the number of possible assignments with ionization energies lower than 10.49 eV also increases. For these higher order masses, which include m/z = 42, 45, 54, 56, 60, 68, 70, 84, and 96, computational calculations that generate intermediates and products on potential energy surfaces can be used to predict likely candidates for each mass-to-charge. These are detailed in the *Discussion* along with proposed reaction mechanisms for all QMS and ReTOF products.

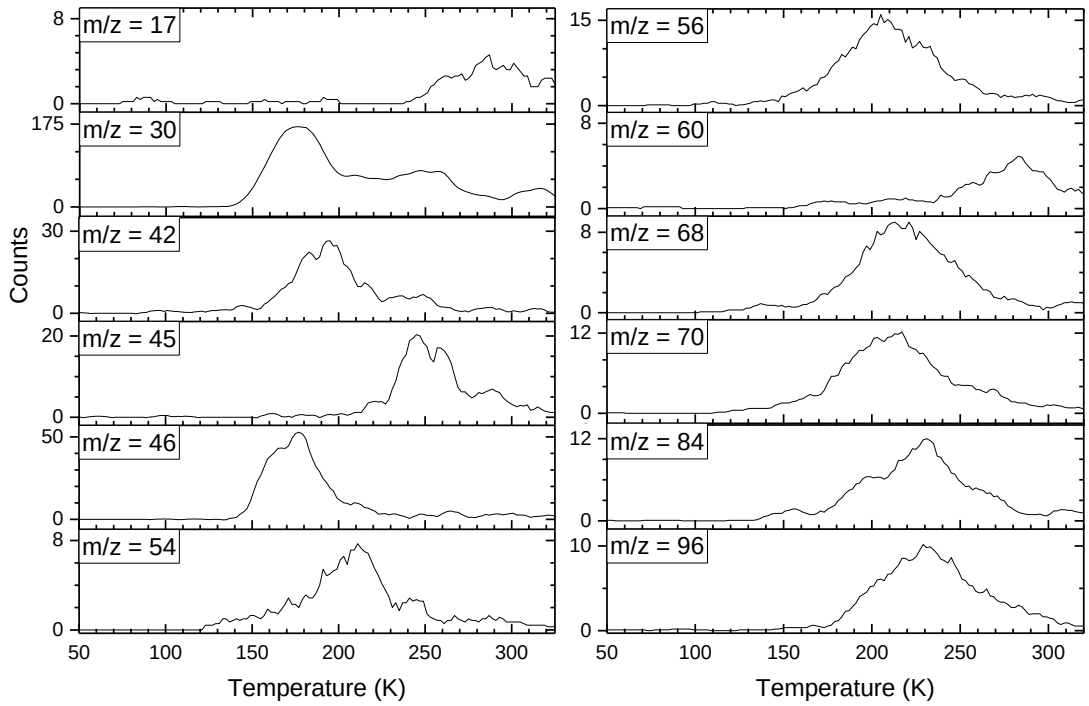

Figure 6. TPD profiles for signals recorded using ReTOF-MS.

4. DISCUSSION

By merging previous computational and new experimental findings, we are proposing now reaction mechanisms for the detected products (Figure 7). A detailed discussion on the formation of nitric oxide (NO) in irradiated solid FOX-7 was previously reported.[42] This study revealed FOX-7 first underwent nitro-to-nitrite isomerization from C–NO_2 to C–ONO (Figure 7, Reaction 1) prior to bond cleavage liberating the NO molecule (Reaction 2). This study also revealed reaction pathways toward the production of nitrogen dioxide (NO_2) and ammonia (NH_3). For nitrogen dioxide, two viable pathways were found. First, the C–NO_2 bond could simply cleave (300 kJ mol^{-1}, Reaction 3) resulting in NO_2 and the corresponding radical fragment, which can undergo hydrogen transfer from a nitrogen atom to the carbon radical (Reaction 4) that stabilizes the FOX-7 fragment by 101 kJ mol^{-1}. Second, a FOX-7 molecule can overcome an initial reaction barrier of 203 kJ mol^{-1} to transfer the hydrogen atom from the nitrogen to the carbon atom with simultaneous release of a nitro group to form nitrogen dioxide

(NO_2) and results in the same FOX-7 remnant as the previous pathway. Similarly, breakage of the C–NH_2 bond (461 kJ mol^{-1}, Reaction 5) provides an amino radical (NH_2) that can combine with a hydrogen atom to form ammonia (Reaction 6), which is exothermic by −444 kJ mol^{-1}.[57]

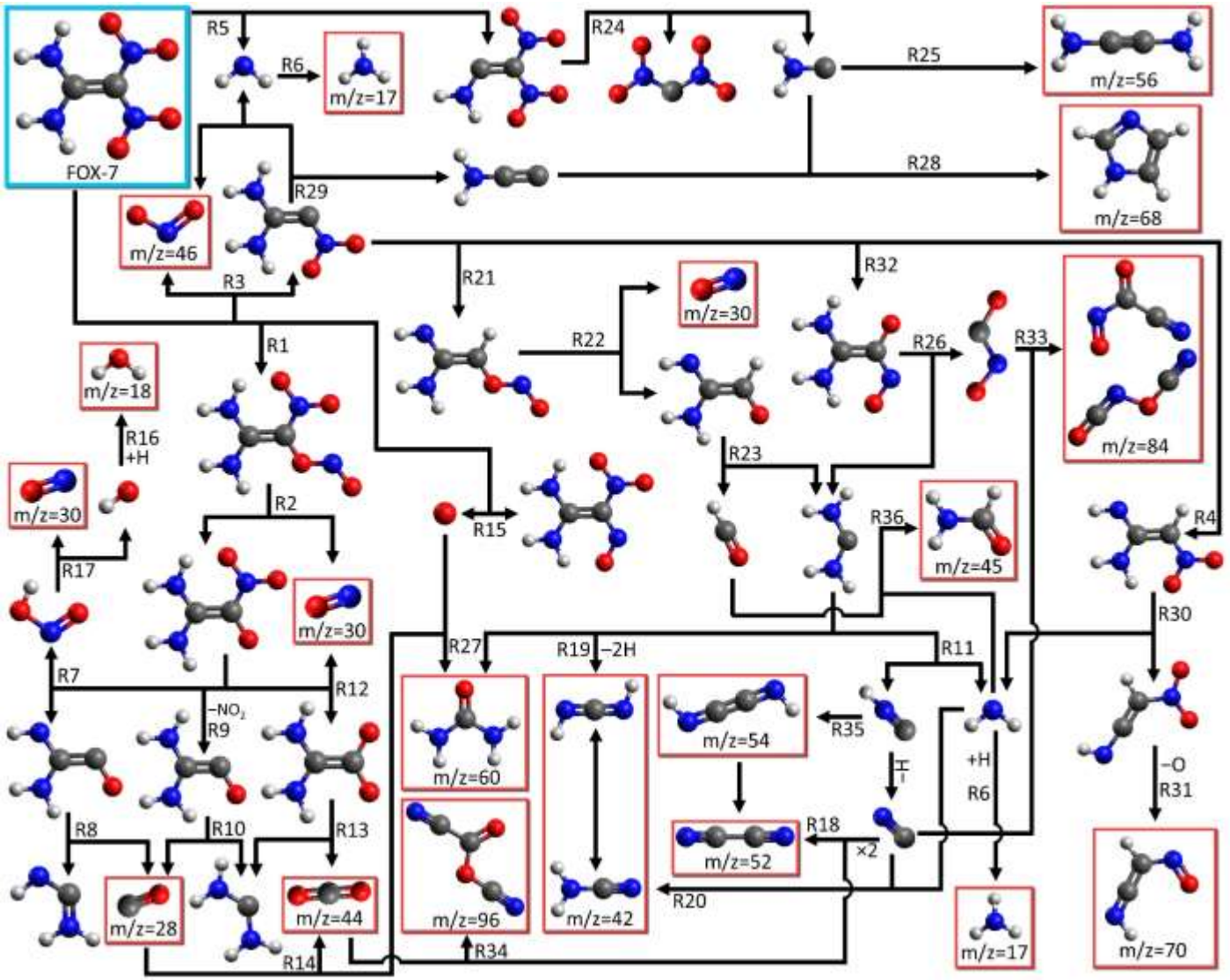

Figure 7. Reaction schemes from FOX-7 (top) showing decomposition pathways toward observed products (red boxed with mass-to-charge ratio). The pathway for Reaction 1 is labeled R1, etc.

Experimentally detected carbon monoxide (CO) has been shown to result from the decomposition of FOX-7 after nitro-to-nitrite isomerization (Reaction 1) followed by NO elimination (Reaction 2). Two mechanisms include a hydrogen migration and subsequent cleavage (112 kJ mol^{-1}) of the remaining nitro group as nitrous acid (HONO, Reaction 7) leaving a $NH_2(NH)CCO$ fragment that further decomposes into an amino radical (NH_2), hydrogen isocyanide (HNC), and carbon monoxide.[20,25] A second pathway without prior hydrogen atom shift shows the remaining nitro group can separate (169 kJ mol^{-1}) forming NO_2 and leaving $(NH_2)_2CCO$ (Reaction 9), which can eliminate CO through a transition state of 62 kJ mol^{-1} (Reaction 10).[25] The diaminocarbene ($C(NH_2)_2$) fragment can further decompose to hydrogen isocyanide (HNC) and NH_2 (Reaction 11), which can combine once again with hydrogen to form ammonia according to Reaction 6. Other variations of these pathways, such as an earlier loss of an amino (NH_2) or nitro (NO_2) group, have been presented with appropriate energetics,[25] but in each case the critical step toward carbon monoxide generation is nitro-to-nitrite isomerization in order to create a carbon-oxygen bond and detachment of this CO moiety from the remaining FOX-7 fragment during decomposition.

The production of experimentally detected carbon dioxide (CO_2) follows from two proposed routes. The first route returns to the previously discussed FOX-7 fragment that remains after nitro-to-nitrite isomerization and NO loss (Reaction 2). Here, the fragment undergoes a *second* nitro-to-nitrite isomerization through a 151 kJ mol^{-1} transition state that, after subsequent NO loss (Reaction 12), results in a $(NH_2)_2CCO_2$ plus NO pair that is 133 kJ mol^{-1} more stable than the initial FOX-7 fragment. Breaking the carbon-carbon bond (Reaction 13) (63 kJ mol^{-1}) results in a free carbon dioxide molecule with the diaminocarbene ($C(NH_2)_2$) fragment.[25] A second route that must be considered is the reaction of carbon monoxide with atomic oxygen (Reaction 14), which is liberated from FOX-7 with a net cost of 346 kJ mol^{-1} (Reaction 15), that has been shown to produce carbon dioxide releasing 526 kJ mol^{-1}.[58-60]

Like ammonia, water can be generated from a radical decomposition product of FOX-7 (in this case, the hydroxyl (OH) radical) that is capable of hydrogen abstraction[35] and/or recombines with a hydrogen atom (−492 kJ mol^{-1}, Reaction 16).[61] Multiple reaction pathways have been proposed that lead to the release of a hydroxyl radical, but the primary ones commence with a transfer of a

hydrogen atom, which can be an inter- or intramolecular transfer, to an oxygen on the nitro (NO_2) group. This transfer can occur both before or after the nitro group has been severed from the FOX-7 molecule, but in both cases a free nitrous acid (HONO, as shown in Reaction 7) molecule results that decomposes (Reaction 17) to the hydroxyl radical (OH) and nitric oxide (NO).[29] This process can even occur after an initial nitro-to-nitrite isomerization followed by NO release (Reaction 2). Here, an intramolecular hydrogen can transfer to the nitro group through a 16 kJ mol^{-1} transition state to form the –NOOH moiety, which could then directly cleave the N–OH bond (184 kJ mol^{-1}) to produce an OH radical, or first nitrous acid (HONO) could separate (112 kJ mol^{-1}, Reaction 7) from the FOX-7 fragment with subsequent N–OH bond rupture (197 kJ mol^{-1}, Reaction 17).[25]

While hydrogen cyanide (HCN) and hydrogen isocyanide (HNC) have been widely reported and predicted as decomposition products of FOX-7,[20,25,31-32] it is notable that our experiment only detects cyanogen (NCCN). Cyano radicals (CN) were reported using laser breakdown spectroscopy by the electronic transition of CN at 388 nm,[33] and the proposed formation of CN radicals includes the reaction of atomic nitrogen, which results from complete decomposition of nitric oxide (NO), with any carbon-containing species to form CN, or from the decomposition of HCN.[33] Hydrogen cyanide (HCN) itself is in equilibrium with hydrogen isocyanide (HNC), which is a decomposition product through various pathways of the amine portion (R-$C(NH_2)_2$) of FOX-7 (Reaction 11). Two cyano radicals can recombine to generate cyanogen (−565 kJ mol^{-1}, Reaction 18).[62]

The CH_2N_2 molecule observed at m/z = 42 has been shown to result from molecular hydrogen loss of the diaminocarbene ($C(NH_2)_2$) fragment through a 221 kJ mol^{-1} transition state and is overall endothermic by 7 kJ mol^{-1} (Reaction 19). The $C(NH)_2$ isomer also exists in equilibrium with its more stable tautomer, cyanamide (NH_2CN), which could form from radical-radical recombination between previously discussed amino (NH_2) and cyano (CN) radicals (Reaction 20).

Starting with m/z = 45, uniquely assigning mass-to-charge ratios becomes more challenging as computational studies failed to locate complex decomposition products. Not only does this complicate the assignment of a molecular formula, but an isomer-specific assignment is more daunting. Therefore, the most expedient method for assigning these masses is to consider the FOX-

7 decomposition fragments that have been identified in the experimental and computational literature as well as potential additional fragments that could form by one bond cleavage and assemble these fragments using radical-radical recombination to ascertain a proposed molecular assignment. This strategy proposes possible products, which have to be verified in follow up studies as discussed below. For example, m/z = 45 can be assigned using the simple molecular formula CH_3NO. While NO (nitric oxide) is a common decomposition fragment of FOX-7, neither the methyl radical (CH_3) nor a methyl group has been identified on reaction schemes of FOX-7 decomposition and thus a reaction of NO and CH_3 is not considered as a possible route toward the formation of CH_3NO. However, the amino radical (NH_2) is also a common decomposition fragment (e.g., Reactions 5 & 11) and requires a formyl (HCO) radical to form a molecule with formula CH_3NO. This can be found on a reaction pathway that initially loses a nitro group (NO_2, Reaction 3). After hydrogen migration to the carbon radical resulting in $NH_2(NH)CCHNO_2$, this fragment stabilizes by 158 kJ mol^{-1} by nitro-to-nitrite isomerization (Reaction 21) and NO separation (Reaction 22) through a transition state of 131 kJ mol^{-1} to produce $NH_2(NH)CCHO$.[25] Cleavage of the carbon-carbon bond (Reaction 23) provides a formyl radical (CHO) that, when combined with an available NH_2 radical, produces formamide (NH_2CHO) with m/z = 45 (Reaction 36).

The $C_2H_2N_2$ formula satisfies the assignment for m/z = 54, and the proposed isomer for this detection is ethenediimine (HNCCNH, Reaction 35).[63] While nitrosyl cyanide (ONCN) may have formed from the recombination of ubiquitous nitric oxide (NO) with a cyano radical (CN), its ionization energy of 10.9 eV[64] means that this molecule would not be ionized at 10.49 eV and thus could not contribute to the signal observed at m/z = 56. Furthermore, butene (C_4H_6) is not considered as the literature has not demonstrated such capacity for the near-complete hydrogenation of carbon atoms during decomposition of FOX-7. Instead, the formula $C_2H_4N_2$ is proposed as the molecular assignment for m/z = 56. The H_2NC fragment has been identified on multiple reaction pathways after near complete destruction of the FOX-7 molecule[25] and could also be formed by carbon-nitrogen bond cleavage of the common H_2NCNH_2 / $HNCNH_2$ intermediates or from carbon-carbon bond cleavage of the amino-loss fragment of FOX-7 (Reaction 5 to Reaction 24). The recombination of two H_2NC fragments (Reaction 25) provides H_2NCCNH_2, diaminoacetylene, for the proposed isomer representing m/z = 56.

For the signal at m/z = 60, two contributions are considered. First, nitric oxide (NO) is known to exist as a dimer in the solid state,[65-66] and while the signal for NO was predominantly seen using QMS and ReTOF at m/z = 30, a fraction of nitric oxide may have remained in the dimer form shortly after sublimation to be detected at m/z = 60 using the ReTOF. The second proposed contribution to m/z = 60 is from the formula CH_4N_2O. Breaking the carbon-carbon bond of FOX-7 results in the common diaminocarbene fragment ($C(NH_2)_2$) (e.g., Reactions 23 & 26), and the reaction of this fragment with an oxygen atom separated from a nitro group (NO_2, Reaction 15) results in carbonyl diamide, $(NH_2)_2CO$, commonly known as urea (Reaction 27).

Given the abundance of oxides of carbon (CO and CO_2) as irradiation products, the possibility of higher order carbon oxides such as tricarbon dioxide (OCCCO) presents an intriguing reaction product for m/z = 68. However, with an ionization energy of 10.60 eV[67], signal from C_3O_2 would not be observed at a photon energy of 10.49 eV. Similarly, the formula C_2N_2O would provide several opportunities to consider reaction mechanisms of small product molecules. However, the C_2N_2O isomers cyanogen isocyanate (NCNCO, IE = 11.49 eV),[68] cyanogen *N*-oxide (ONCCN, IE = 11.32 eV),[69] and dicyano ether (NCOCN, IE = 12.69 ± 0.05 eV) also have ionization energies too high to be ionized with 10.49 eV photons and would not contribute to the m/z = 68 signal. Therefore, the proposed molecular formula assigned to m/z = 68 is $C_3H_4N_2$, represented by the cyclic imidazole molecule (c-NCHCHNHCH), which can form from the recombination of the CNH_2 and $CCNH_2$ radicals followed by hydrogen migration (Reaction 28). The CNH_2 radical has been shown to result from multiple reaction pathways involving carbon-carbon bond breakage (Reaction 24) and the loss of one amino group (NH_2, Reaction 5).[25] The $CCNH_2$ radical could form from a single bond dissociation from one of several predicted intermediates: H_2NCCNO_2, $H_2NCCONO$, or H_2NCCO, and the process is ultimately represented by the loss of both nitro groups (NO_2) and one amino group (NH_2) from FOX-7 (Reaction 29).

While the signal at m/z = 70 could belong to one of several molecular formulas, the best assignment using the available FOX-7 fragments is $C_2H_2N_2O$. Several isomers can be considered for this formula: cyanoformamide ($NH_2C(O)CN$), furazan (1,2,5-oxadiazole, c-CHNONCH), 1,3,4-oxadiazole (c-CHNNCHO), hydroxyimino-acetonitrile (HONCHCN), nitroso-ethenimine,

nitroso-acetonitrile ($ONCH_2CN$). The unknown ionization energies for these isomers were calculated (*Supporting Information*) and presented in Tables S2–S4. The cyanoformamide (11.15 eV), furazan (11.32 eV), hydroxyimino-acetonitrile (10.87 eV) and 1,3,4-oxadiazole (10.77 eV) isomers have calculated ionization energies too high to be ionized at 10.49 eV. Therefore, the possible assignments for m/z = 70 include nitroso-acetonitrile (10.01 eV) and nitroso-ethenimine (8.16 eV), which could be interconverted by one hydrogen shift. The best candidate for nitroso-ethenimine formation involves the $HNCCHNO_2$ fragment that was computed after FOX-7 lost a nitro group (NO_2, Reaction 3)) and underwent a hydrogen shift to $H_2N(NH)CCHNO_2$ (Reaction 4). An additional 195 kJ mol^{-1} of energy cleaved the amino group (NH_2) leaving the $HNCCHNO_2$ fragment (Reaction 30). A loss of an oxygen atom results in nitroso-ethenimine (Reaction 31).

Multiple molecular formulas could reasonably be considered for the signal at m/z = 84. The first proposed formula is $C_2N_2O_2$ and has six acyclic isomers that include three symmetric chains (ONCCNO, NCOOCN, and OCNNCO), two asymmetric chains (OCNOCN and ONNCCO), and one branched isomer (ONC(O)CN). While numerous cyclic isomers also exist, nearly all of them are highly unstable, but the most plausible cyclic representative is the five-membered c-CNC(O)ON. The most promising precursors leading to these isomers include the decomposition intermediates ONCOH and OCNOH, which only differ by a hydrogen shift. These intermediates originate from the $(NH_2)_2CC$ (O)NO fragment that formed after initial NO_2 loss from FOX-7 resulting in the $(NH_2)_2CCNO_2$ radical (Reaction 3) followed by a migration of an oxygen atom through a 153 kJ mol^{-1} transition state to form $(NH_2)_2CC(O)NO$ (Reaction 32). While hydrogen shifts followed by carbon-carbon bond cleavage eventually lead to ONCOH and OCNOH, breaking the carbon-carbon bond first would produce the nitroformyl radical (ONCO, Reaction 26), which was first detected in an electron-irradiated matrix of nitrogen (N_2) and carbon dioxide at 10 K.[70] Of the possible $C_2N_2O_2$ isomers mentioned, only OCNOCN and ONC(O)CN contain the ONCO moiety and both are the product of ONCO recombining with a cyano (CN) radical (Reaction 33). Besides $C_2N_2O_2$, $C_2H_4N_4$ is a potential formula that could explain the m/z = 84 signal. While many isomers exist, a notable compound with this formula is 2-cyanoguanidine ($(NH_2)_2CNCN$). Although diaminocarbene ($C(NH_2)_2$) is a known decomposition product of FOX-7, the cyanonitrene (NCN) counter-fragment has not yet been detected nor explored computationally in FOX-7 studies and thus remains a potential decomposition product if, for

example, $C(NH_2)_2$ were stripped of hydrogens during decomposition leaving only the NCN backbone.

The highest mass-to-charge ratio observed was m/z = 96; of the many possible molecular formulae, the one that best represents the known decomposition products is $C_3N_2O_2$. At least 10 acyclic isomers of varying stability exist, but most require intermediates that are plausible but not yet observed during FOX-7 decomposition nor computationally considered. These fragments include the CCO and OCN moieties that, while not computationally identified as discrete intermediates, exist in portions of larger intermediates. A proposed isomer of $C_3N_2O_2$ formed with identified species is cyano(oxo)methyl cyanate (NCC(O)OCN) and can be formed by the combination of carbon dioxide (CO_2) and two cyano radicals (CN, Reaction 34).

The rate constants for the decomposition of FOX-7 as well as the production of carbon monoxide (CO) and carbon dioxide (CO_2) can be utilized to better understand the importance of relevant reactions in Figure 7. Note that while Figure 4 shows an asymptotic decrease of key functional groups of FOX-7 (C=C, -NO_2, and -NH) that all have leveled off near 84 % of their original intensity, the *rate* at which these functional groups reach the same ultimate destination is distinct. The fastest decay occurs with the amino group (NH_2), which has a rate constant (2.1×10^{-3} s^{-1}) three times as large as C=C (6.8×10^{-4} s^{-1}) and 60 % larger than the NO_2 decrease. That the amino group (NH_2) reacts so rapidly favors reaction pathways such as Reaction 5, which cleaves the C-NH_2 bond and releases NH_2, over pathways such as Reaction 3, which separates the nitro group (NO_2) from FOX-7. While Reaction 29, which is consecutive to Reaction 3, also eliminates a NH_2 group, FOX-7 would first need to cleave a NO_2 group during Reaction 3, and thus Reaction 5 is favored over Reaction 29 for the removal of NH_2 groups. The intermediate reaction rate is the decline of the -NO_2 functional group. After Reaction 5, a nitro group (NO_2) could be removed from the remaining fragment, or Reaction 3 may proceed as depicted but at a slower rate than Reaction 5. The carbon-carbon stretching vibration displayed the slowest reaction rate indicating that FOX-7 likely did not proceed with a fast initial split of the FOX-7 molecule into $C(NH_2)_2$ and $C(NO_2)_2$ components. Indeed, the calculated potential energy surfaces did not find such a reaction that led to the observed products and thus this reaction is not presented in Figure 7. Instead, multiple amino (NH_2) or nitro (NO_2) groups are eliminated from FOX-7 before

carbon-carbon bond cleavage occurs, which explains the slow rate of decay. Rate constants were also determined for carbon monoxide (CO) and carbon dioxide (CO_2) production and found that the rate constant for CO production was nearly three times higher than for CO_2. The reaction pathways to generate these products are similar. Both processes require a nitro-to-nitrite isomerization (Reaction 1) followed by elimination of nitric oxide (NO, Reaction 2). Carbon monoxide (CO) then proceeds through -NO_2 cleavage (Reaction 9) and separates from the remaining $C(NH_2)_2$ fragment (Reaction 10). The route to carbon dioxide (CO_2) though must first undergo a second nitro-to-nitrite isomerization with NO elimination (Reaction 12). Like with the carbon monoxide (CO) reaction pathway, carbon dioxide (CO_2) is then formed by the loss of $C(NH_2)_2$ (Reaction 13). The key difference in these pathways is the second nitro-to-nitrite isomerization step required to form CO_2, and isomerization of the (second) nitro group (NO_2) (Reaction 12) may be slower than bond cleavage to remove it (Reaction 9). However, Reactions 12 and 13 may not be the dominant reaction pathway to carbon dioxide (CO_2) and instead Reaction 14, in which carbon monoxide (CO) reacts with an oxygen atom, may be the preferred route to CO_2 formation. This pathway could explain the observed absence of molecular oxygen signals (m/z = 32) compared to photolysis studies[42]. In the case of electron irradiation, additional products such a carbon monoxide can scavenge any newly generated atomic oxygen and serve as an oxygen sink that prevents the formation of molecular oxygen. This has been shown to occur to electron-irradiated ices of carbon monoxide (CO) which found that carbon monoxide reacts with atomic oxygen to form carbon dioxide (CO_2, Reaction 14).[59]

5. CONCLUSIONS

The electron irradiation of a solid FOX-7 sample at 5 K was designed to study the decomposition products and non-thermal reaction mechanisms. Infrared spectroscopy only detected carbon dioxide (CO_2) and carbon monoxide (CO), but found that about 16 % of the FOX-7 sample had reacted, which is in agreement with CASINO simulations. During irradiation and TPD, the QMS detected water (H_2O), nitric oxide (NO), carbon monoxide (CO), carbon dioxide (CO_2), and cyanogen (NCCN). Quantitative yields using FTIR and QMS data showed that less than 1 % of the reacted FOX-7 carbon remained trapped in the matrix as CO or CO_2 awaiting

sublimation during TPD, although the overall signal during irradiation indicated that about 4 % of the reacted carbon converting to CO or CO_2. PI-ReTOF-MS also detected small molecules such as ammonia (NH_3), nitric oxide (NO), and nitrogen dioxide (NO_2). More complex molecules could have multiple molecular formulas that would satisfy the observed mass-to-charge ratio, but using experimentally and computationally identified intermediates and products, molecular and isomeric assignments were proposed for each signal along with reaction mechanisms to form these isomers. While the utilization of previous computations was necessary for describing reaction pathways, we note that the fragments formed, in particular the oxygen and hydrogen atoms, are born under non-equilibrium conditions. This even may involve excited states such as for atomic oxygen, which was demonstrated in the decomposition of nitromethane (CH_3NO_2), which is a model compound often used by the energetics material science community.[71-76] These non-equilibrium conditions and the generation of suprathermal atoms can result in reaction pathways where entrance barriers can be overcome easily.[77] All these reaction mechanisms highlight the importance of the nitro-to-nitrite isomerization that allowed carbon-oxygen bonds to form and nitric oxide (NO) to be released. Additionally, diaminocarbene ($C(NH_2)_2$) was a major precursor toward many products by providing the cyano species (CN, HCN, HNC) along with an amino radical (NH_2). Future experiments exploiting isotopically-labeled FOX-7, such as ^{13}C-FOX-7, could lend mass spectrometric support to the assignment of the molecular formulae of larger molecules through isotope shifts in the QMS and PI-ReTOF-MS data. Once accomplished, experiments utilizing tunable photoionization can provide further selections of the remaining isomers using experimental or calculated ionization energies. The determination of reaction rate constants using FTIR intensities indicated that the amino group (NH_2) was lost most rapidly, followed by the nitro group (NO_2). Only after several of these outer functional groups had been eliminated could carbon-carbon bond dissociation occur, which was the slowest observed process. The results are generally in good agreement with previous studies but also included new products not yet identified using other methods while also finding that some common products are absent with this technique. This emphasizes the differences in methodologies and shows the importance of confirming computational results, that are often limited to gas phase molecules or small clusters, with experimental observations of solid samples capable of suppressing thermal reactions.

ASSOCIATED CONTENT

Supporting Information

Infrared assignments of FOX-7 from 500 – 6000 cm^{-1}, calculated ionization energies, geometries, and infrared bands for $H_2C_2N_2O$ isomers.

ACKNOWLEDGMENTS

The Hawaii groups acknowledge support from the Office of Naval Research (A9550-21-1-0221).

References

1. Fried, L. E.; Manaa, M. R.; Lewis, J. P., In *Overviews of Recent Research on Energetic Materials*, Shaw, R. W.; Brill, T. B.; Thompson, D. L., Eds. World Scientific Publishing: Singapore, 2005; pp 275-301.
2. Oxley, J. C., In *Theoretical and Computational Chemistry*, Politzer, P.; Murray, J. S., Eds. Elsevier: New York, 2003; Vol. 12, pp 5-48.
3. Kozak, G. D. Factors Augmenting the Detonability of Energetic Materials. *Propellants, Explos., Pyrotech.* **2005,** *30*, 291-297.
4. Singh, R. P.; Verma, R. D.; Meshri, D. T.; Shreeve, J. M. Energetic Nitrogen-Rich Salts and Ionic Liquids. *Angew. Chem., Int. Ed.* **2006,** *45*, 3584-3601.
5. Sikder, A. K.; Sikder, N. A Review of Advanced High Performance, Insensitive and Thermally Stable Energetic Materials Emerging for Military and Space Applications. *J. Hazard. Mater.* **2004,** *112*, 1-15.
6. Badgujar, D. M.; Talawar, M. B.; Asthana, S. N.; Mahulikar, P. P. Advances in Science and Technology of Modern Energetic Materials: An Overview. *J. Hazard. Mater.* **2008,** *151*, 289-305.
7. Adams, G. F.; Shaw, R. W. Chemical Reactions in Energetic Materials. *Annu. Rev. Phys. Chem.* **1992,** *43*, 311-340.
8. Brill, T. B.; James, K. J. Kinetics and Mechanisms of Thermal Decomposition of Nitroaromatic Explosives. *Chem. Rev.* **1993,** *93*, 2667-2692.
9. Behrens, R., In *Overviews of Recent Research on Energetic Materials*, Shaw, R. W.; Brill, T. B.; Thompson, D. L., Eds. World Scientific Publishing: Singapore, 2005; pp 29-73.
10. Sorescu, D. C.; Boatz, J. A.; Thompson, D. L. Classical and Quantum-Mechanical Studies of Crystalline FOX-7 (1,1-Diamino-2,2-Dinitroethylene). *J. Phys. Chem. A* **2001,** *105*, 5010-5021.
11. Majano, G.; Mintova, S.; Bein, T.; Klapötke, T. M. Confined Detection of High-Energy-Density Materials. *J. Phys. Chem. C* **2007,** *111*, 6694-6699.
12. Mathieu, D. Mateo: A Software Package for the Molecular Design of Energetic Materials. *J. Hazard. Mater.* **2010,** *176*, 313-322.
13. Shteinberg, A. S.; Berlin, A. A.; Denisaev, A. A.; Mukasyan, A. S. Kinetics of Fast Reactions in Condensed Systems: Some Recent Results (an Autoreview). *Int. J. Self-Propag. High-Temp. Synth.* **2011,** *20*, 259-265.
14. Morton, R. J.; Kaiser, R. I. Kinetics of Suprathermal Hydrogen Atom Reactions with Saturated Hydrides in Planetary and Satellite Atmospheres. *Planet. Space Sci.* **2003,** *51*, 365-373.
15. Singh, S. K.; La Jeunesse, J.; Vuppuluri, V.; Son, S. F.; Sun, B.-J.; Chen, Y.-L.; Chang, A. H. H.; Mebel, A. M.; Kaiser, R. I. The Elusive Ketene (H_2CCO) Channel in the Infrared Multiphoton Dissociation of Solid 1,3,5-Trinitro-1,3,5-Triazinane (RDX). *ChemPhysChem* **2020,** *21*, 837-842.
16. Singh, S. K.; Vuppuluri, V.; Son, S. F.; Kaiser, R. I. Investigating the Photochemical Decomposition of Solid 1,3,5-Trinitro-1,3,5-Triazinane (RDX). *J. Phys. Chem. A* **2020,** *124*, 6801-6823.
17. Latypov, N. V.; Bergman, J.; Langlet, A.; Wellmar, U.; Bemm, U. Synthesis and Reactions of 1,1-Diamino-2,2-Dinitroethylene. *Tetrahedron* **1998,** *54*, 11525-11536.

18. Yuan, B.; Yu, Z.; Bernstein, E. R. Initial Decomposition Mechanism for the Energy Release from Electronically Excited Energetic Materials: FOX-7 (1,1-Diamino-2,2-Dinitroethene). *J. Chem. Phys.* **2014,** *140*, 074708.
19. Booth, R. S.; Butler, L. J. Thermal Decomposition Pathways for 1,1-Diamino-2,2-Dinitroethene (FOX-7). *J. Chem. Phys.* **2014,** *141*, 134315.
20. Gindulyte, A.; Massa, L.; Huang, L.; Karle, J., In *Theoretical and Computational Chemistry*, Politzer, P.; Murray, J. S., Eds. Elsevier: New York, 2003; Vol. 12, pp 91-109.
21. Jiang, L.; Fu, X.; Zhou, Z.; Zhang, C.; Li, J.; Qi, F.; Fan, X.; Zhang, G. Study of the Thermal Decomposition Mechanism of FOX-7 by Molecular Dynamics Simulation and Online Photoionization Mass Spectrometry. *RSC Adv.* **2020,** *10*, 21147-21157.
22. Kimmel, A. V.; Sushko, P. V.; Shluger, A. L.; Kuklja, M. M. Effect of Charged and Excited States on the Decomposition of 1,1-Diamino-2,2-Dinitroethylene Molecules. *J. Chem. Phys.* **2007,** *126*, 234711.
23. Politzer, P.; Concha, M. C.; Grice, M. E.; Murray, J. S.; Lane, P. Computational Investigation of the Structures and Relative Stabilities of Amino/Nitro Derivatives of Ethylene. *J. Mol. Struct.: THEOCHEM* **1998,** *452*, 75-83.
24. Türker, L.; Varış, S. Effects of Epoxidation and Nitration on Ballistic Properties of FOX-7 – a DFT Study. *Z. Anorg. Allg. Chem.* **2013,** *639*, 982-987.
25. Luo, Y.; Kang, C.; Kaiser, R.; Sun, R. The Potential Energy Profile of the Decomposition of 1,1-Diamino-2,2-Dinitroethylene (FOX-7) in the Gas Phase. *Phys. Chem. Chem. Phys.* **2022,** *24*, 26836-26847.
26. Rashkeev, S. N.; Kuklja, M. M.; Zerilli, F. J. Electronic Excitations and Decomposition of 1,1-Diamino-2,2-Dinitroethylene. *Appl. Phys. Lett.* **2003,** *82*, 1371-1373.
27. Zong, H.; Huang, Y.; Shu, Y.; Wang, X. Theoretical Study on the Initial Thermal Decomposition and Catalysis Effects of NO_2 on FOX-7. *Hanneng Cailiao* **2006,** *14*, 425-428.
28. Zheng, Z.; Xu, J.; Zhao, J. First-Principles Studies on the Thermal Decomposition Behavior of FOX-7. *High Pressure Res.* **2010,** *30*, 301-309.
29. Liu, Y.; Li, F.; Sun, H. Thermal Decomposition of FOX-7 Studied by Ab Initio Molecular Dynamics Simulations. *Theo. Chem. Acc.* **2014,** *133*, 1567.
30. Ma, Y.; Lv, M.; Shang, F.; Zhang, C.; Liu, J.; Zhou, P. Mechanistic Investigation on the Initial Thermal Decomposition of Energetic Materials FOX-7 and RDX in the Crystal and Gas Phase: An MM/DFT-Based Oniom Calculation. *J. Phys. Chem. A* **2022,** *126*, 1666-1673.
31. Jones, D.; Vachon, M.; Wang, R.; Kwok, Q. In *Preliminary Studies on the Thermal Properties of FOX-7*, Proceeding NATAS Annu. Conf. Therm. Anal. Appl. 32nd, 2004; pp 1-105.
32. Jin, P.-G.; Chang, H.; Chen, Z.-Q. Studies on Kinetics and Mechanisms of Thermal Decomposition of 1, 1-Diamino-2, 2-Dinitroethylene (FOX-7). *Baozha Yu Chongji* **2006,** *26*, 528.
33. Civiš, M.; Civiš, S.; Sovová, K.; Dryahina, K.; Španěl, P.; Kyncl, M. Laser Ablation of FOX-7: Proposed Mechanism of Decomposition. *Anal. Chem.* **2011,** *83*, 1069-1077.
34. Winey, J. M.; Zimmerman, K.; Dreger, Z. A.; Gupta, Y. M. Structural Transformation and Chemical Stability of a Shock-Compressed Insensitive High Explosive Single Crystal: Time-Resolved Raman Spectroscopy. *J. Phys. Chem. A* **2020,** *124*, 6521-6527.
35. Zhang, J.-D.; Zhang, L.-L. Theoretical Study on the Mechanism of the Reaction of FOX-7 with OH and NO_2 Radicals: Bimolecular Reactions with Low Barrier During the Decomposition of FOX-7. *Mol. Phys.* **2017,** *115*, 2951-2960.

36. Li, J.; Zhou, T.; Chen, J.; Wang, X.; Wang, Y.; Liu, W.; Zhang, X.; Li, Z.; Chen, X.; Han, J. Theoretical Studies on 2,3,5,6-Tetra (1H-Tetrazol-5-yl) Pyrazine and 1,1-Diamino-2,2-Dinitroethylene Blending System. *J. Mol. Grpahics Modell.* **2022,** 108235.
37. Banik, S.; Yadav, A. K.; Kumar, P.; Ghule, V. D.; Dharavath, S. Unfolding the Chemistry of FOX-7: Unique Energetic Material and Precursor with Numerous Possibilities. *Chem. Eng. J.* **2021,** 133378.
38. Ghosh, M.; Sikder, A. K.; Banerjee, S.; Talawar, M. B.; Sikder, N. Preparation of Reduced Sensitivity Co-Crystals of Cyclic Nitramines Using Spray Flash Evaporation. *Def. Technol.* **2020,** *16*, 188-200.
39. Krisyuk, B. E.; Sypko, T. M. Mechanism of Thermolysis of Hydrazino-Dinitroethylenes. *Comput. Theor. Chem.* **2022,** *1211*, 113662.
40. Shang, F.; Wang, T.; Ma, Y.; Lv, M. Theoretical Study on Several Important Decomposition Paths of FOX-7 and Its Derivatives. *Comput. Theor. Chem.* **2022,** *1217*, 113895.
41. Nazin, G.; Dubikhin, V.; Kazakov, A.; Nabatova, A.; Krisyuk, B.; Volkova, N.; Shastin, A. Kinetics of the Decomposition of 1, 1-Diamino-2, 2-Dinitroethylene (FOX-7). Part 4: Comparison of the Decomposition Reactions of FOX-7 and Its Diazacyclic Derivatives. *Russ. J. Phys. Chem. B* **2022,** *16*, 308-315.
42. Turner, A. M.; Luo, Y.; Marks, J. H.; Sun, R.; Lechner, J. T.; Klapötke, T. M.; Kaiser, R. I. Exploring the Photochemistry of Solid 1,1-Diamino-2,2-Dinitroethylene (FOX-7) Spanning Simple Bond Ruptures, Nitro-to-Nitrite Isomerization, and Nonadiabatic Dynamics. *J. Phys. Chem. A* **2022,** *126*, 4747-4761.
43. Turner, A. M.; Bergantini, A.; Koutsogiannis, A. S.; Kleimeier, N. F.; Singh, S. K.; Zhu, C.; Eckhardt, A. K.; Kaiser, R. I. A Photoionization Mass Spectrometry Investigation into Complex Organic Molecules Formed in Interstellar Analog Ices of Carbon Monoxide and Water Exposed to Ionizing Radiation. *Astrophys. J.* **2021,** *916*, 74.
44. Kaiser, R. I. Experimental Investigation on the Formation of Carbon-Bearing Molecules in the Interstellar Medium Via Neutral-Neutral Reactions. *Chem. Rev.* **2002,** *102*, 1309-1358.
45. Jones, B. M.; Kaiser, R. I. Application of Reflectron Time-of-Flight Mass Spectroscopy in the Analysis of Astrophysically Relevant Ices Exposed to Ionization Radiation: Methane (CH_4) and D_4-Methane (CD_4) as a Case Study. *J. Phys. Chem. Lett.* **2013,** 1965-1971.
46. Turner, A. M.; Kaiser, R. I. Exploiting Photoionization Reflectron Time-of-Flight Mass Spectrometry to Explore Molecular Mass Growth Processes to Complex Organic Molecules in Interstellar and Solar System Ice Analogs. *Acc. Chem. Res.* **2020,** *53*, 2791-2805.
47. Latypov, N. V.; Johansson, M.; Holmgren, E.; Sizova, E. V.; Sizov, V. V.; Bellamy, A. J. On the Synthesis of 1,1-Diamino-2,2-Dinitroethene (FOX-7) by Nitration of 4,6-Dihydroxy-2-Methylpyrimidine. *Org. Process Res. Dev.* **2007,** *11*, 56-59.
48. Astrat'ev, A. A.; Dashko, D. V.; Mershin, A. Y.; Stepanov, A. I.; Urazgil'deev, N. A. Some Specific Features of Acid Nitration of 2-Substituted 4,6-Dihydroxypyrimidines. Nucleophilic Cleavage of the Nitration Products. *Russ. J. Org. Chem.* **2001,** *37*, 729-733.
49. Hilbig, R.; Wallenstein, R. Narrowband Tunable VUV Radiation Generated by Nonresonant Sum-and Difference-Frequency Mixing in Xenon and Krypton. *Appl. Opt.* **1982,** *21*, 913-917.
50. Hovington, P.; Drouin, D.; Gauvin, R. Casino: A New Monte Carlo Code in C Language for Electron Beam Interaction—Part I: Description of the Program. *Scanning* **1997,** *19*, 1-14.
51. Bouilloud, M.; Fray, N.; Bénilan, Y.; Cottin, H.; Gazeau, M.-C.; Jolly, A. Bibliographic Review and New Measurements of the Infrared Band Strengths of Pure Molecules at 25 K: H_2O,

CO_2, CO, CH_4, NH_3, CH_3OH, HCCOH and H_2CO. *Mon. Not. R. Astron. Soc.* **2015,** *451*, 2145-2160.
52. Bennett, C. J.; Jamieson, C.; Mebel, A. M.; Kaiser, R. I. Untangling the Formation of the Cyclic Carbon Trioxide Isomer in Low Temperature Carbon Dioxide Ices. *Phys. Chem. Chem. Phys.* **2004,** *6*, 735-746.
53. Jones, B. M.; Kaiser, R.; Strazzulla, G. UV-Vis, Infrared, and Mass Spectroscopy of Electron Irradiated Frozen Oxygen and Carbon Dioxide Mixtures with Water. *Astrophys. J.* **2014,** *781*, 85-96.
54. Bennett, C. J.; Ennis, C. P.; Kaiser, R. I. Implantation of Energetic D^+ Ions into Carbon Dioxide Ices and Implications for Our Solar System: Formation of D_2O and D_2CO_3. *Astrophys. J.* **2014,** *794*, 57.
55. Turner, A. M.; Abplanalp, M. J.; Chen, S. Y.; Chen, Y. T.; Chang, A. H.; Kaiser, R. I. A Photoionization Mass Spectroscopic Study on the Formation of Phosphanes in Low Temperature Phosphine Ices. *Phys. Chem. Chem. Phys.* **2015,** *17*, 27281-27291.
56. Electron-Impact Ionization Cross Sections. Physical Measurement Laboratory, Nist. Accessed 2022. https://www.nist.gov/pml.
57. Harding, M. E.; Vázquez, J.; Ruscic, B.; Wilson, A. K.; Gauss, J.; Stanton, J. F. High-Accuracy Extrapolated Ab Initio Thermochemistry. III. Additional Improvements and Overview. *J. Chem. Phys.* **2008,** *128*, 114111.
58. Bennett, C. J.; Jamieson, C. S.; Kaiser, R. I. Mechanistical Studies on the Formation of Carbon Dioxide in Extraterrestrial Carbon Monoxide Ice Analog Samples. *Phys. Chem. Chem. Phys.* **2009,** *11*, 4210-4218.
59. Bennett, C. J.; Jamieson, C. S.; Kaiser, R. I. An Experimental Investigation of the Decomposition of Carbon Monoxide and Formation Routes to Carbon Dioxide in Interstellar Ices. *Astrophys. J. Suppl. Ser.* **2009,** *182*, 1.
60. Active Thermochemical Tables, Argonne National Laboratory. Accessed 2023. https://atct.anl.gov/
61. Maksyutenko, P.; Rizzo, T. R.; Boyarkin, O. V. A Direct Measurement of the Dissociation Energy of Water. *J. Chem. Phys.* **2006,** *125*, 181101.
62. Huang, Y.; Barts, S. A.; Halpern, J. B. Heat of Formation of the Cyanogen Radical. *J. Phys. Chem.* **1992,** *96*, 425-428.
63. Jobst, K. J.; Hanifa, M. R.; Terlouw, J. K. The Covalently Bound HNC Dimer Ion $HNCCNH^+$ Has a Kinetically Stable Neutral Counterpart. *Chem. Phys. Lett.* **2008,** *462*, 152-157.
64. Jonkers, G.; Mooyman, R.; De Lange, C. Ultraviolet Photoelectron Spectroscopy of Unstable Species: Nitrosyl Cyanide (ONCN). *Chem. Phys.* **1981,** *57*, 97-104.
65. Góbi, S.; Crandall, P. B.; Maksyutenko, P.; Förstel, M.; Kaiser, R. I. Accessing the Nitromethane (CH_3NO_2) Potential Energy Surface in Methanol (CH_3OH)–Nitrogen Monoxide (NO) Ices Exposed to Ionizing Radiation: An FTIR and PI-ReTOF-MS Investigation. *J. Phys. Chem. A* **2018,** *122*, 2329-2343.
66. Fateley, W. G.; Bent, H. A.; Crawford Jr, B. Infrared Spectra of the Frozen Oxides of Nitrogen. *J. Chem. Phys.* **1959,** *31*, 204-217.
67. Baker, C.; Turner, D. The Photoelectron Spectrum and Ionisation Potentials of Carbon Suboxide. *Chem Commun* **1968,** 400-401.
68. Frost, D.; Kroto, H.; McDowell, C.; Westwood, N. The HeI Photoelectron Spectra of the Isoelectronic Molecules, Cyanogen Azide, NCN_3, and Cyanogen Isocyanate, NCNCO. *J. Electron Spectrosc. Relat. Phenom.* **1977,** *11*, 147-156.

69. Pasinszki, T.; Westwood, N. P. C. Ground, Excited, and Ionic States of the NCCNO Molecule: A HeI Photoelectron, Infrared, Ultraviolet, and Ab Initio Investigation. *J. Phys. Chem.* **1996,** *100*, 16856-16863.
70. Jamieson, C. S.; Mebel, A. M.; Kaiser, R. I. A Matrix Isolation Study of the C_s Symmetric OCNO (X^2A'') Radical. *Phys. Chem. Chem. Phys.* **2005,** *7*, 4089-4095.
71. Singh, S. K.; Kaiser, R. I. A Vacuum Ultraviolet Photoionization Study on the Isomerization, Decomposition, and Molecular Mass Growth Processes in Solid Nitromethane (CH_3NO_2). *Chem. Phys. Lett.* **2021,** *766*, 138343.
72. Maksyutenko, P.; Forstel, M.; Crandall, P.; Sun, B.-J.; Wu, M. H.; Chang, A. H. H.; Kaiser, R. I. An Isomer-specific Study of Solid Nitromethane Decomposition Pathways - Detection of Aci-nitromethane ($H_2CNO(OH)$) and Nitrosomethanol ($HOCH_2NO$) Intermediates. *Chem. Phys. Lett.* **2016**, *658*, 20-29.
73. Tsegaw, Y. A.; Sander, W.; Kaiser, R. I. Electron Paramagnetic Resonance Spectroscopic Study on Nonequilibrium Reaction Pathways in the Photolysis of Solid Nitromethane (CH_3NO_2) and D3-Nitromethane (CD_3NO_2). *J. Chem. Phys. A* **2016,** *120*, 1577-1587.
74. Kaiser, R. I.; Maksyutenko, P. Novel Reaction Mechanisms Pathways in the Electron Induced Decomposition of Solid Nitromethane (CH_3NO_2) and D3-Nitromethane (CD_3NO_2). *J. Phys. Chem. C* **2015**, *119*, 14653-14668.
75. Kaiser, R. I.; Maksyutenko, P. A Mechanistical Study on Non-Equilibrium Reaction Pathways in Solid Nitromethane (CH_3NO_2) and D3-Nitromethane (CD_3NO_2) upon Interaction with Ionizing Radiation. *Chem. Phys. Lett.* **2015**, *631-632*, 59-65.
76. Maksytenko, P.; Muzangwa, L. G.; Jones, B. M.; Kaiser, R. I. Lyman α Photolysis of Solid Nitromethane (CH_3NO_2) and D3-Nitromethane (CD_3NO_2) - Untangling the Reaction Mechanisms Involved in the Decomposition of Model Energetic Materials. *Phys. Chem. Chem. Phys.* **2015**, *17*, 7514-7527 (2015).
77. Morton, R. J.; Kaiser, R. I. Kinetics of Suprathermal Hydrogen Atom Reactions with Saturated Hydrides in Planetary and Satellite Atmospheres. *Planet. Space Sci.* **2003**, *51*, 365-373.

TOC

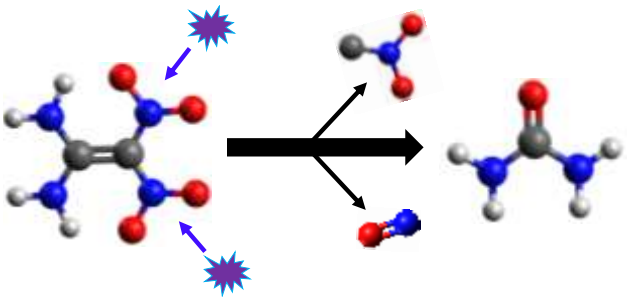

Supporting Information

Electron-Induced Decomposition of Solid 1,1-Diamino-2,2-Dinitroethylene (FOX-7) at Cryogenic Temperatures

Andrew M. Turner,[a,b] Joshua H. Marks,[a,b] Yuheng Luo,[a] Jasmin T. Lechner,[c] Thomas M. Klapötke,[c] Rui Sun,[a] Ralf I. Kaiser [a,b*]

[a] *Department of Chemistry, University of Hawaii, Honolulu, HI 96822, USA*

[b] *W. M. Keck Research Laboratory in Astrochemistry, University of Hawaii, Honolulu, HI 96822, USA*

[c] *Department of Chemistry, Ludwig-Maximilian University of Munich, 81377 München, Germany*

*ralfk@hawaii.edu

Table S1. Experimental infrared band positions of FOX-7 compared to previous values.

Mode	This work (cm^{-1})	Thin Layer[a] (cm^{-1})	Powder[a] (cm^{-1})	Assignment[a]
1	3442	3425		$\nu_{as}(NH_2)$
2	3411	3406	3402	$\nu_{as}(NH_2)$
3	3337	3333	3329	$\nu_{s}(NH_2)$
4	3313	3298	3295	$\nu_{s}(NH_2)$
5	1649	1633	1632	$\nu_{s}(C–NH_2)$
6	1606	1608	1605	$\delta_{s}(NH_2)$
7	1525	1523	1520	$\delta_{s}(NH_2)$
8	1498	1503		$\nu(C–C)$
	1470	1470	1470	$\nu_{17} + \nu_{24}$
	1450			
9	1383	1392	1390	$\nu(C–C)$
10	1352	1352	1350	$\nu_{as}(NO_2)$
11	1311	1312		$\rho(NH_2)$, $\nu_{s}(C–NO_2)$
	1261			$\rho(NH_2)$, $\nu_{as}(C–NO_2)$
12	1228	1221	1212	
13	1178	1169	1166	$\rho(NH_2)$, $\nu_{s}(NO_2)$
14	1145	1141	1140	$\rho(NH_2)$, $\nu_{s}(NO_2)$
15	1068	1063		$\rho(NH_2)$
16	1038	1025	1022	$\rho(NH_2)$
17	862	858	857	$\delta_{s}(NO_2)$
18	771	790	789	$\tau(NH_2)$
19	748	751	749	$\delta_{s}(NO_2)$
20	737	739	738	$\delta(C{-}NO_2)$, $\tau(NH_2)$
21	679	674	673	$\delta(C{-}NO_2)$, $\tau(NH_2)$
22		644		$\omega(NH_2)$
23		635	636	$\tau(NH_2)$
24	623	620	617	$\tau(NH_2)$

Notes:

[a] Data and assignments from Turner et al. 2022. Thin layer solid sample recorded under UHV conditions and powdered sample spectrum obtained at ambient conditions

Computational Methods

The adiabatic ionization energies (IE) were calculated as the energy difference between the vibrational ground state of the neutral molecules and their corresponding cations. The geometries and unscaled zero-point energies (ZPEs) of the neutral molecules and cations were calculated with dispersion-corrected density functional theory (DFT-D3) M06-2X-D3[1-2] with the triple-zeta basis set def2-TZVPP[3] in NWChem (Version 6.8.1).[4] The energies of optimal geometries were refined at open-shell unrestricted explicitly correlated couple-cluster single and double excitations and a perturbative treatment of triple excitations (UCCSD(T)-F12A/cc-pVTZ-F12) level with molecular orbitals from restricted Hartree–Fock (RHF) calculations[5-9] in Molpro (Version 2021.2),[10-11] which followed the same scheme as the previous FOX-7 studies.[12-13] In addition, to deal with the convergence issue of open-shell cations (i.e., $[NH_2CHO]^+$, $[(NH_2)_2CO]^+$, $[(NH_2C(O)CN)]^+$) in RHF calculations, DFT calculations were performed and used as initial orbitals guess for RHF calculations.

Table S2: Calculated ionization energies with ZPE for $H_2C_2N_2O$ isomers.

Name	Ionization Energy (eV)	Relative Energy (kJ mol^{-1})	Structure[a]
furazan	11.32	225	
cyanoformamide	11.15	0	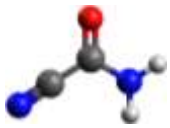
hydroxyimino-acetonitrile	10.87–11.10	203–228	
1,3,4-oxadiazole	10.77	89	
nitroso-acetonitrile	10.01–10.03	267–272	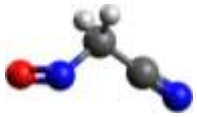
nitroso-ethenimine	8.16	342–349	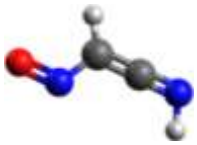

Notes:

[a]Calculated coordinates for molecules and any conformers are presented below.

Table S3. Geometries (in Angstroms) underlying the calculated energies for $H_2C_2N_2O$ isomers in Table

Atom	X	Y	Z	Atom	X	Y	Z
		Furazan				Cyanoformamide	
C	-0.69622658	-0.89376894	0.00000171	C	0.12875695	0.47517591	-0.00000001
C	0.72387103	-0.8714897	-0.00000387	N	-1.09438882	1.04415481	-0.00000002
N	-1.11906798	0.32978834	0.00000043	H	-1.15380297	2.04865068	0.00000000
H	-1.38321181	-1.72143206	0.00000007	H	-1.9333551	0.49214343	0.00000001
N	1.10825593	0.36465177	0.00000363	C	0.06607435	-1.00970495	0.00000005
H	1.43613991	-1.67754729	0.00000037	O	1.18009369	1.05405946	0.00000000
O	-0.01723681	1.10347289	-0.00000232	N	0.01972324	-2.15357	-0.00000003
		Hydroxyimino-acetonitrile (1)				Hydroxyimino-acetonitrile (2)	
C	-0.08670633	0.45708339	0.00000224	C	-0.05129826	0.42472094	0.0012764
C	1.34203698	0.33772847	-0.00000072	C	1.373929	0.27200148	-0.00418468
N	-0.77912785	-0.60538839	0.00000158	N	-0.77889216	-0.61528609	-0.00007374
H	-0.53328223	1.44652947	0.00000002	H	-0.45058528	1.43883364	0.0079634
N	2.48763713	0.29925905	-0.00000064	N	2.51850667	0.21308136	-0.00555756
O	-2.11259096	-0.32774001	-0.00000155	O	-2.1117975	-0.42380336	0.01005416
H	-2.5331872	-1.19244626	-0.00000093	H	-2.3165793	0.52499136	0.02496172
		Hydroxyimino-acetonitrile (3)				Hydroxyimino-acetonitrile (4)	
C	0.9094352	-0.1912535	-0.1039424	C	0.96995924	-0.22302126	-0.10817763
C	0.31614256	1.10252993	0.10082638	C	0.39529555	1.08121834	0.08748916
N	0.25220425	-1.27447511	-0.18060013	N	0.2594171	-1.27653079	-0.19642957
H	1.98285213	-0.26066147	-0.20006355	H	2.04070202	-0.33290935	-0.18526261
N	-0.11547142	2.15207023	0.26213862	N	-0.14637057	2.08098706	0.24361353
O	-1.08812419	-1.09150745	-0.04967795	O	-1.07357518	-1.16487713	-0.10321641
H	-1.45574136	-1.9774825	-0.11558226	H	-1.33833808	-0.23701342	0.0282677
		nitroso-acetonitrile (1)				nitroso-acetonitrile (2)	
C	-0.5286916	0.83282234	0.01817874	C	-0.1575047	0.60878321	0.00971365
C	0.91228557	0.62925543	0.00634299	C	1.27514399	0.35263873	0.00025403
N	-1.34534426	-0.43908705	0.00805929	N	-0.93804419	-0.69761161	0.01261249
N	2.04311508	0.45199914	-0.00060069	N	2.40097823	0.14666921	-0.00748305
O	-0.7090711	-1.43112161	-0.03284445	O	-2.10041139	-0.49344438	-0.01858379
H	-0.8572843	1.3974648	-0.85515352	H	-0.46091031	1.17407495	-0.87100038
H	-0.84575148	1.38067632	0.90582856	H	-0.44788065	1.16117477	0.90326183
		nitroso-ethenimine (1)				nitroso-ethenimine (2)	
H	-0.46741836	2.86206263	-0.74627589	H	-0.40108236	2.60911621	-0.42777616
N	-0.24302739	2.31191135	0.07793212	O	-1.14351572	-1.18953419	-0.02926919
C	0.13149513	1.17700048	-0.02448991	C	0.42359521	0.91786795	0.03426328
O	-0.03914522	-2.19687395	0.03118573	N	-0.05527755	1.98364611	0.29343332
H	1.58852343	-0.35478597	-0.04632498	H	1.95589854	-0.50767012	-0.22888189
N	-0.46495798	-1.0713853	0.028209	N	0.03109976	-1.43129285	-0.11491412
C	0.54224499	-0.0836862	-0.01398477	C	0.90434878	-0.309901	-0.11470937
		1,3,4-oxadiazole					
N	-0.66446809	-0.98155704	0.0000032				
N	0.72590868	-0.9370897	-0.00000451				
C	-1.05484938	0.23705743	-0.00000109				
C	1.03751011	0.30402126	0.00000458				
O	-0.03583943	1.11956711	-0.00000165				
H	-2.06045777	0.61833974	-0.00000013				
H	2.01670498	0.74877384	-0.0000004				

S2.

Table S4. Calculated infrared band positions (in cm^{-1}) for $H_2C_2N_2O$ isomers presented in Table S2.

Normal Modes	Furazan	Cyano-formamide	Hydroxyimino-acetonitrile (1)	(2)	(3)	(4)	Nitroso-acetonitrile (1)	(2)	Nitroso-ethenimine (1)	(2)	1,3,4-oxadiazole
ν_1	673	204	215	209	193	177	191	145	167	177	660
ν_2	675	294	222	216	327	336	227	207	212	311	694
ν_3	894	312	482	497	438	490	390	389	521	472	884
ν_4	940	501	487	504	484	542	436	519	546	528	915
ν_5	964	576	540	541	647	658	768	541	609	629	967
ν_6	982	633	588	585	756	767	778	894	730	812	972
ν_7	1019	776	962	930	904	881	895	904	875	839	1038
ν_8	1063	784	1059	1078	993	999	1008	1019	897	861	1144
ν_9	1097	1123	1117	1125	1076	1086	1221	1210	1092	974	1173
ν_{10}	1222	1354	1302	1331	1345	1348	1312	1312	1121	1152	1250
ν_{11}	1384	1620	1452	1473	1403	1480	1439	1430	1391	1357	1346
ν_{12}	1503	1857	1743	1710	1749	1681	1787	1773	1652	1657	1592
ν_{13}	1635	2421	2425	2426	2419	2402	2434	2438	2170	2160	1610
ν_{14}	3294	3614	3179	3124	3243	3252	3108	3105	3227	3285	3314
ν_{15}	3315	3738	3872	3709	3874	3664	3146	3154	3547	3560	3324

References

1. Zhao, Y.; Truhlar, D. G., The M06 Suite of Density Functionals for Main Group Thermochemistry, Thermochemical Kinetics, Noncovalent Interactions, Excited States, and Transition Elements: Two New Functionals and Systematic Testing of Four M06-Class Functionals and 12 Other Functionals. *Theo. Chem. Acc.* **2008,** *120* (1), 215-241.

2. Grimme, S.; Antony, J.; Ehrlich, S.; Krieg, H., A Consistent and Accurate Ab Initio Parametrization of Density Functional Dispersion Correction (Dft-D) for the 94 Elements H-Pu. *J. Chem. Phys.* **2010,** *132* (15), 154104.

3. Weigend, F.; Ahlrichs, R., Balanced Basis Sets of Split Valence, Triple Zeta Valence and Quadruple Zeta Valence Quality for H to Rn: Design and Assessment of Accuracy. *Phys. Chem. Chem. Phys.* **2005,** *7* (18), 3297-3305.

4. Valiev, M.; Bylaska, E. J.; Govind, N.; Kowalski, K.; Straatsma, T. P.; Van Dam, H. J. J.; Wang, D.; Nieplocha, J.; Apra, E.; Windus, T. L.; de Jong, W. A., Nwchem: A Comprehensive and Scalable Open-Source Solution for Large Scale Molecular Simulations. *Comp. Phys. Comm.* **2010,** *181* (9), 1477-1489.

5. Raghavachari, K.; Trucks, G. W.; Pople, J. A.; Head-Gordon, M., A Fifth-Order Perturbation Comparison of Electron Correlation Theories. *Chem. Phys. Lett.* **1989,** *157* (6), 479-483.

6. Knowles, P. J.; Hampel, C.; Werner, H. J., Coupled Cluster Theory for High Spin, Open Shell Reference Wave Functions. *J. Chem. Phys.* **1993,** *99* (7), 5219-5227.

7. Adler, T. B.; Knizia, G.; Werner, H.-J., A Simple and Efficient Ccsd(T)-F12 Approximation. *J. Chem. Phys.* **2007,** *127* (22), 221106.

8. Peterson, K. A.; Adler, T. B.; Werner, H.-J., Systematically Convergent Basis Sets for Explicitly Correlated Wavefunctions: The Atoms H, He, B–Ne, and Al–Ar. *J. Chem. Phys.* **2008,** *128* (8), 084102.

9. Knizia, G.; Adler, T. B.; Werner, H.-J., Simplified Ccsd(T)-F12 Methods: Theory and Benchmarks. *J. Chem. Phys.* **2009,** *130* (5), 054104.

10. Werner, H. J.; Knowles, P. J.; Knizia, G.; Manby, F. R.; Schütz, M., Molpro: A General-Purpose Quantum Chemistry Program Package. *Wiley Interdisciplinary Reviews: Computational Molecular Science* **2012,** *2* (2), 242-253.

11. Werner, H.-J.; Knowles, P. J.; Manby, F. R.; Black, J. A.; Doll, K.; Heßelmann, A.; Kats, D.; Köhn, A.; Korona, T.; Kreplin, D. A.; Ma, Q.; MillerIII, T. F.; Mitrushchenkov, A.; Peterson, K. A.; Polyak, I.; Rauhut, G.; Sibaev, M., The Molpro Quantum Chemistry Package. *The Journal of Chemical Physics* **2020,** *152* (14), 144107.

12. Luo, Y.; Kang, C.; Kaiser, R.; Sun, R., The Potential Energy Profile of the Decomposition of 1,1-Diamino-2,2-Dinitroethylene (Fox-7) in the Gas Phase. *Physical Chemistry Chemical Physics* **2022,** *24* (43), 26836-26847.

13. Turner, A. M.; Luo, Y.; Marks, J. H.; Sun, R.; Lechner, J. T.; Klapötke, T. M.; Kaiser, R. I., Exploring the Photochemistry of Solid 1,1-Diamino-2,2-Dinitroethylene (Fox-7) Spanning Simple Bond Ruptures, Nitro-to-Nitrite Isomerization, and Nonadiabatic Dynamics. *The Journal of Physical Chemistry A* **2022,** *126* (29), 4747-4761.